Journal of Thermal Analysis and Calorimetry (2021) 145:1075–1090
https://doi.org/10.1007/s10973-020-10413-7

Thermodynamic analysis and multi-objective optimization performance of solid oxide fuel cell–Ericsson heat engine–reverse osmosis desalination

Omolbanin Shakouri[1] · Mamdouh El Haj Assad[2] · Emin Açıkkalp[3]

Received: 29 June 2020 / Accepted: 15 November 2020 / Published online: 4 January 2021

Abstract

This paper targets to consider a hybrid cycle consisting of a solid oxide fuel cell and an Ericsson thermal engine that provides drinking water by connecting to a reverse osmosis desalination unit. First, a parametric assessment was performed on the target functions, including power, exergy destruction density, and fresh water production. After conducting studies on the composition of these target functions, three scenarios are defined for the simultaneous optimization of the mentioned functions. The first scenario targets to optimize the exergy destruction density (Exd) and the fresh water production (m_f). In this scenario the exergy destruction and fresh water production have a better condition in the FUZZY approach, that the maximum value of the exergy destruction density and fresh water production are 450.879 (W m^{-2}) and 2.078 (kg s^{-1}), respectively. The second scenario attempts to optimize the power (P) and the fresh water production (m_f). According this scenario the power has the highest value in the FUZZY that is equal to 531.965 (KW), besides the fresh water production achieves to a maximum value in TOPSIS which it value is 0.365 (kg s^{-1}). The third scenario considers optimizing the power (P), the fresh water production (m_f), and the exergy destruction density (Exd). The power (P) has permanent value in three decision-making which is equal 311.105 (KW), also the fresh water production (m_f) is 1.816 (kg s^{-1}) in three decision-making and besides the exergy destruction density (Exd) has a constant value in three decision-making which is 30.439 (W m^{-2}). In all three scenarios, the decision-making methods, such as TOPSIS, FUZZY, and LINMAP were appropriate to specify the ultimate solution between the beam fronts.

Keywords Solid oxide fuel cell · Reverse osmosis desalination · Ericsson engine · Irreversibility · Exergy destruction density · Energy and exergy efficiencies · Multi-objective optimization

Introduction

Nowadays, the situation of energy consumption in the world is increasing. Therefore, many studies have been done in the field of thermodynamic analysis of energy systems [1–3]. Grisolia et al. [1] investigated new indicator for the analysis of sustainability and thermodynamic optimization. Lucia et al. [2] considered the sustainability and thermodynamic assessment of land system according to new indicator. Arabkoohsar et al. [3] investigate thermodynamics, thermodynamic assessment of a hybrid thermal. Today, fuel cells are a good field of study for many of researchers and engineers due to their high operating temperatures. In this regard, as well as modeling a solid oxide fuel cell using two methods of mass and distributed modeling was presented [4]. Nafees et al. [5] have studied the simulation of natural gas power in a solid oxide fuel cell; the results show that

✉ Mamdouh El Haj Assad
massad@sharjah.ac.ae

✉ Emin Açıkkalp
eacikkalp@gmail.com

Omolbanin Shakouri
f.shakuri070@gmail.com

[1] Faculty of Mechanical and Mechatronics Engineering, Shahrood University of Technology, Shahrood, Iran

[2] Sustainable and Renewable Energy Engineering Department, University of Sharjah, P O Box 27272, Sharjah, UAE

[3] Department of Mechanical Engineering, Engineering Faculty, Bilecik S.E. University, Bilecik, Turkey

using an advanced SOFC simulation, in turn, optimizes the performance of the SOFC and its applications. In the field of solid oxide fuel cells, it can be studied the materials used in solid oxide fuel cells [6], as well as a brief description of the operation, design, manufacturing process, and performance of solid oxide fuel cells [7, 8]. Zacearia et al. [9] have studied the power of advanced gas turbine systems to improve the economic durability of solid oxide fuel cells, according to the results of flexibility by turbines; gas has increased the lifespan of solid oxide fuel cells and improved system performance. Research on the progress of solid oxide fuel cells [10]. Shichuan Su et al. [11] indicated a different design of the cell on the performance of solid oxide fuel cells. According the results, although by increasing width, CSC and Asc cells performance decrease, but Asc cells have a greater impact on SOFC performance due to better design. Beigzadeh et al. [12] have examined simple modeling of a SOFC energy system powered by natural gas, the result of effect voltage and efficiency on pressure and temperature of fuel cell. Zhao et al. [13] studied a new analytical approach for modeling and evaluating the performance of a type of irreversible fuel cell. The results provide real theoretical foundations for the optimal design and operation of solid oxide fuel cells (SOFC) that are a good field of study for many researchers today. Solid oxide fuel cell (SOFC) is suitable for hybrid systems due to its high operating temperature. In this regard, Açıkkalp et al. [14] analyze the performance of the solid oxide fuel cell–heat engine of Brighton based on an environmental thermo-criterion, the results of which are numerically expressed for all parameters. Xu et al. [15] studied the performance of the direct carbon solid oxide fuel cell (DC-SOFC) and the ironing motor. According to the results, the ironing motor can heat the fuel cell waste (DC-SOFC) to generate power at high current densities. Zhao et al. [16] have optimized the thermal engine hybrid system, the fuel cell, and designed its index parameters. Zhang et al. [17] analyzed the performance of the hybrid system, including the irreversible fuel cell–thermal engine. Zhang et al. [18] proposed a new analytical method to evaluate and optimize the performance of the irreversible solid oxide fuel cell fuel system and gas turbine. Zhang et al. [19] investigated the effect of irreversible damage on the performance of the combined solid oxide fuel cell and molten carbon gas and the results show that using molten carbonate fuel cells will increase the power and combined system efficiency. Chen et al. [20] analyzed the performance and optimization of multi-targets of the Sterling thermal engine hybrid system and the irreversible solid oxide fuel cell. The results show that the performance of the solid oxide fuel cell can be greatly increased by connecting the sterling thermal engine to increase power generation. According to the existing combined systems Gholamian et al. [21] studied a combined system of solid oxide fuel cell (SOFC) with a sterling engine for aviation use and the results show that in a combined system including SOFC and sterling engine, the temperature increases the system exergy efficiency. Rokni et al. [22] investigated the thermodynamic system of solid oxide fuel cell (SOFC) and a Stirling engine for heat production and combined power (CHP) with pure electric capacity 120 KWe. The results of this study show that the pressure and temperature of the solar cells increase the voltage and efficiency of the cell, and current increasing reduces the voltage of the cells. Rokni et al. [23] evaluated the hybrid power system (10 kW) for a residential home. The system is powered by a solid oxide fuel cell (SOFC) on top of Stirling engine and the output gas products of the cycle are fed by a sterling engine and produce additional power in the engine. The results show that the combined system improves the overall electrical efficiency of an independent sterling engine or a solid oxide fuel cell (SOFC) system. Mehrpooya and et al. [24] investigated the operation of a specific kind of heating system.

Today, Ericsson and Sterling engines have attracted the attention of many engineers and physicists because of their high efficiency and using different types of fluid work that in recent years, Ericsson cycles have been widely used in electro thermodynamic converters that in this field, Tyagi et al. [25] evaluated the thermodynamic optimization and parametric study of an irreversible Ericsson heat engine with limited heat capacity for external tanks. Chen et al. [26] examined the comprehensive impact of several irreversible factors, including heat transfer at the same rate, reduction losses, and heat leakage on the performance of the Ericsson heat engine. The results show that in a heat transfer at a constant speed, reduction processes are affected by thermal resistance on the Erickson and Sterling cycles. Hachem et al. [27] investigated a compare and a specific kind of Stirling engine, the outcomes demonstrate similar parameters Stirling and Ericsson engine, environmental optimization, and study of engines function of irreversible thermal engines of Ericsson and Sterling [28]. Ngangue et al. [29] worked on the dynamic simulation of a liquid piston with an Ericsson engine; the results show that as the rotational speed increases, the efficiency of the motor decreases. FULA et al. [30] performed indoor cylinder heat transfer on a prime example of an Ericsson engine, so the results indicate that Ericsson engines are more efficient than fossil fuels for the conversion of solar energy to micro-CHP systems due to the production of external heat than fossil fuels that have attracted the attention of many engineers. Bădescu et al. [31] optimized the use of a solar converter combined with an Ericsson or Sterling thermal engine. The results show that the combined systems of the solar collector-thermal engine will have the optimum temperature. Erbay et al. [32] also examined an irreversible internal Ericson engine with a real resuscitator, according to the results, by increasing the efficiency of the turbine and

compressor cycle the power and density reduce. Durcansky et al. [33] designed a heat exchanger for hot air from the Ericsson-Brighton piston engine; the results show that using simultaneous production systems is a good solution for using energy more. Kussul et al. [34] have studied Ericson's microchannel heat engine for solar concentrators with flat mirrors. According to the results, the Ericsson engine can be used to convert the thermal energy of a solar concentrator into mechanical energy. The Ericsson engine is a thermal engine driven by external heat [35].

Recently countless studies have been implemented on multi-objective optimizing of different heat engines which led to different analyses of output power and heat efficiency of the engine [36–38]. Ahmadi et al. [36] studied multi-objective optimization for designing the Stirling heat engine, and according to the results, Sterling engine pressure losses can reach the minimum point by using multi-objective optimization method simultaneously. Ahmadi et al. [37] also investigated multi-objective optimization of the Ericsson engine through an evolutionary algorithm. Punnathanam et al. [38] studied the multi-objective optimization of Sterling engine systems. Today, several kinds of researches have been done on multi-objective optimization on numerous cycles. In this regard, Ahmadi et al. [39] analyzed the evolutionary algorithm thermodynamically based on of multi-objective optimization of the Rankin cycle heat engine. The results show that two target operations including efficiency and power had reached the maximum point of their selves by optimizing. Ahmadi et al. also [40] studied the multi-objective and stable optimization of Bryson's irreversible cycle in nano- scale which operates with Maxwell Boltzmann gas that optimum researches for study targets include maximum available work, biological coefficient function, and energy efficiency for Bryson's irreversible cycle has been determined in nano-scale. Ahmadi et al. [41] analyzed thermodynamic function and multi-objective optimization of the Lenoir reversible heat engine cycle economically. High-tech energy systems are suit opportunity for researchers, because they have high efficiency for efficient energy production and eco-friendly features. Today, multi-objective optimizations have been done on solid oxide fuel cells to develop and operate solid oxide fuel cells (SOFC) better [39, 41]. Behzadi Forough et al. [42] studied the multi-objective optimization of clusters of SOFC based on the effect of fuel and hydrogen cost parameters. Analyzing multi-objective optimization results gives a better and more profound understanding of the effect of optimizing operation situations on system operation. Wu et al. [43] investigated the multi-objective optimization of SOFC wherein the main two goals were to maximize the electric efficiency and minimize the cost. According to outcomes, the recommended method has reached the maximum efficiency and minimum cost of SOFC. Salehi et al. [44] analyzed unclear modeling of multi-objective and optimizing reversible SOFC and the results indicate that in fuel cell operating mode by increasing temperature the density of power will improve. Quddus et al. [45] studied the multi-objective optimizing of SOFC to connect methane oxidative by genetic algorithm and the results show that better and broader distribution makes the resolutions of optimizing SOFC operate better. Today, lots of studies have been done on multi-objective optimization of combined systems due to their high efficiency. In this regard, Khani et al. [46] studied multi-objective optimization of combined systems of SOFC and gas production turbines and the results indicate that optimization is useful for more efficient designing of synchronized production systems. Also, Ahmadi et al. [47] optimized and analyzed a molten carbonate fuel cell and Brayson's heat and as the findings indicate recommended resolutions with the LINMAP method in general, are less sensitive than flow density changes.

Exergy analysis is a significant tool for thermodynamic evaluation of energy systems performance [48, 49]. Selladarai and et al. [48] analyzed the exergy of the hydrocarbon refrigerant mixture of R290/R600a as an another to R134a. Senturk and et al. [49] analysed a solar integrated geothermal Rankine cycle. Murugapoopathi and et al. [50] investigated the energy and exergy of ratio multi-fuel engine with variable compression. Also according study Vakilabadi and et al. [51] analyzed energy and exergy and also investigated the performance of a solar thermal power plant. In addition in these field, Allijanpour and et al. [52] analyzed the thermodynamic of a hybrid system according a specific kind of fuel cell.

In the present work also used of Exergy analysis, which this work is a thermodynamic-electrochemical model composed of a solid oxide fuel cell (SOFC)–Ericsson heat engine–reverse osmosis desalination (RO) hybrid system is appointed. According to this system, the Ericsson heat engine uses the waste heat of SOFC and produce power. Also, utilize the waste heat from the SOFC to achieve higher efficiency in whole hybrid system is provided. The main aim of this paper is to investigate the effects of irreversibilities on the fuel cell efficiency. Furthermore, curry out the multiobjective optimize on the fresh water production (m_f), the exergy destruction density, (Exd) and the power (P) and, achieve to more fresh water. The total simulation of the present paper has been done by MATLAB software.

Model description

Figure 1 schematically demonstrates the entire cycle of solid oxide fuel cell SOFC—Ericsson engine—RO desalination. This blow cycle illustrates a general design of whole process present work

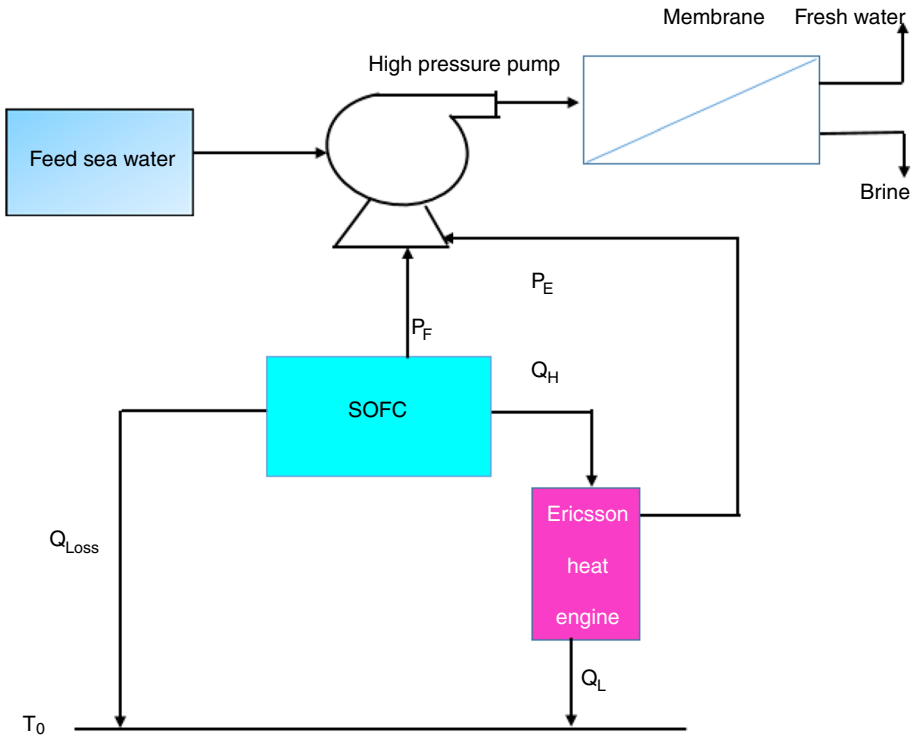

Fig. 1 Schematic the hybrid system presented in this paper

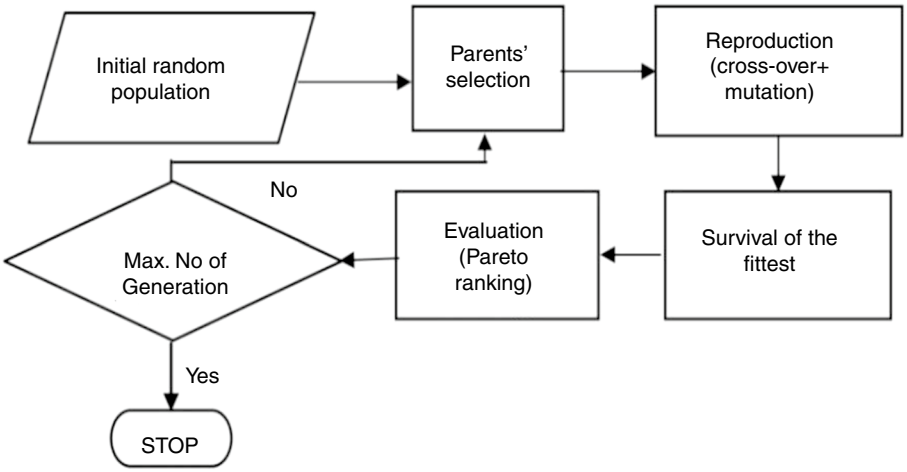

Fig. 2 Algorithm steps applied in the study [39–41]

SOFC model

Fuel cells are proper equipment for energy production from very low capacities to very large power plants because of their high efficiency and non-emission of environmental pollutants. The structure and main body of the fuel cell are made of electrolyte, anode and cathode. A solid oxide fuel cell is an energy converter that theoretically generates electrical energy as long as the oxidizer and fuel are supplied to its electrodes. Of course, practically, friction and corrosion reduce the life of the fuel cell. SOFC (solid oxide fuel cell) technology has many advantages over combustion technologies.

The efficiency and power of the fuel cell are expressed as Eqs. (1) and (2), [13].

$$\eta_F = \frac{P_F}{-\Delta H} = \frac{1}{-\Delta h}\left(m - \frac{k}{\mathrm{RTd}}m^2\right) \tag{1}$$

$$P_F = \frac{iA}{n_e F}\left(m - \frac{k}{\mathrm{RTd}}m^2\right) \tag{2}$$

In Eqs. (1) and (2), the parameter i is defined as current density, F Faraday constant, n_e number of electrons, A surface area of the plate, R constant global gases, and T is the temperature of the solid fuel cell.

m and d equations are described as follows:

$$d = 2n_e \sinh^{-1}\left(\frac{i}{2i_{io,a}}\right) + 2n_e \sinh^{-1}\left(\frac{i}{2i_{o,c}}\right) - \ln\left(1 - \frac{i}{i_{L,a}}\right) - \ln\left(1 - \frac{i}{i_{L,c}}\right) + \frac{in_eFL_{el}}{\sigma_0 R}\exp\left(\frac{E_{el}}{RT}\right) \quad (3)$$

$$m = -\Delta g(T) + RT\ln\left(\frac{P_{H_2}P_{O_2}^{\frac{1}{2}}}{P_{H_2O}}\right) - \mathrm{RTd} \quad (4)$$

In Eqs. (3) and (4), the parameters, $i_{o,a}$ and $i_{o,c}$, are, respectively, the value of the anode and cathode current, L_{el}, the value of the electrode thickness and $i_{L,a}$ and $i_{L,C}$ the sectional currents of anode and cathode, E_{el} is the activation energy and Δg is the change in the function change molar Gibbs.

The enthalpy changes, reversible power, and density of the oxidized fuel cell degradation of the solid oxide are defined according to Eqs. (5), (6), and (7), respectively [13].

$$-\Delta H = -\frac{iA}{n_eF}\Delta h \quad (5)$$

$$P_{F,rev} = -\frac{iA}{n_eF}\Delta g \quad (6)$$

$$\mathrm{Exd}_F = P_{F,rev} - P_F \quad (7)$$

The transform rate of heat regenerator according to Eq. (8) is defined as T_0 environment temperature, K_r is the heat conductance of the regenerator and ε_r *is* regenerator efficiency

$$Q_r = K_r(1 - \varepsilon_r)(T - T_0) \quad (8)$$

Using thermodynamic rule 1, output heat from solid oxide fuel cell is defined as:

$$Q_H = -\Delta H - P_F - Q_r \quad (9)$$

Analysis of the Ericsson engine

The Ericson engine works based on the Ericsson cycle and is also known as an external combustion engine, which is placed between the compressor and the expander to improve the efficiency of the Ericsson engine. The Ericson cycle has four thermodynamic processes of compression, combustion, expansion and heat transfer to the external environment.

In this section, the thermodynamic parameters of the Ericson engine are studied. According to Eqs. (10) and (11), the parameters ε_H *and* ε_L are the effective values of high-temperature and low-temperature heat exchangers, respectively, and also C_H and C_L are defined as the external fluid heat rate of heat source and the heat channel.

$$K_1 = \varepsilon_H C_H \quad (10)$$

$$K_2 = \varepsilon_L C_L \quad (11)$$

Equations (12) and (13) show heat source temperature T_H and heat sync temperature T_C, respectively.

$$T_h = \left[\frac{T_{H1}\sqrt{\frac{K_1}{K_2}} + \sqrt{T_{L1}T_{H1}}}{1 + \sqrt{\frac{K_1}{K_2}}}\right] \quad (12)$$

$$T_C = \left[\frac{T_{L1} + \sqrt{T_{H1}T_{L1}\left(\frac{K_1}{K_2}\right)}}{1 + \sqrt{\frac{K_1}{K_2}}}\right] \quad (13)$$

Changing the fluid entropy in the Ericson engine is defined as follows.

$$\Delta S = nR\ln(\lambda) \quad (14)$$

According to Eq. (14), parameter n is the mole numbers of the heat engine working fluid and λ is the relation of pressure and mass through recovery processes.

$$Y = T_C \quad (15)$$

$$X = \frac{T_h}{T_C} \quad (16)$$

According to Eq. (17), C_f and ε_R are defined parameters of the specific heat of the working fluid in the recovery process and the effectiveness of regenerator, respectively.

$$a_2 = \frac{\mathrm{nc_f}(1 - \varepsilon_R)}{\Delta S} \quad (17)$$

Using Eqs. (14), (16) and (17), Ericson engine efficiency is defined as:

$$\eta_E = \frac{(X-1)}{X\Delta s + a_2(X-1)} \quad (18)$$

According to Eqs. (19) and (20), the amount of heat and output power of the Ericson engine is defined as follows.

$$Q_{\mathrm{L}} = Q_{\mathrm{H}}\left(1 - \eta_{\mathrm{E}}\right) \tag{19}$$

$$P_{\mathrm{E}} = \frac{Q_{\mathrm{H}} - Q_{\mathrm{L}}}{\frac{X\Delta S}{K_1(T_{\mathrm{H1}} - XY)} + \frac{\Delta S}{K_2(Y - T_{\mathrm{L1}})} + 2\alpha(X-1)} \tag{20}$$

The power, efficiency, and density of exergy destruction of the hybrid system are expressed in Eqs. (21)–(23), respectively.

$$P_{\mathrm{h}} = P_{\mathrm{F}} + P_{\mathrm{E}} \tag{21}$$

$$\eta_{\mathrm{h}} = \frac{P_{\mathrm{F}} + P_{\mathrm{E}}}{-\Delta H} \tag{22}$$

$$\mathrm{Exd}_{\mathrm{h}} = \mathrm{Exd}_{\mathrm{F}} + \mathrm{Exd}_{\mathrm{E}} \tag{23}$$

The energy efficiency, exergy, and thermo-environmental function of the hybrid system are expressed in Eqs. (24) and (25), respectively.

$$\varphi_{\mathrm{h}} = \frac{P_{\mathrm{F}} + P_{\mathrm{E}}}{P_{\mathrm{rev,F}} + P_{\mathrm{rev,\,E}}} \tag{24}$$

$$F = \frac{P_{\mathrm{h}}}{Mb_1 + Exd_{\mathrm{h}}b_2 + P_{\mathrm{h}}b_3} \tag{25}$$

Reserve osmosis desalination subsystem

Reverse osmosis desalination system is a technology for water purification. Reverse osmosis using a semi-permeable membrane can remove soluble and suspended particles in water and a variety of bacteria. This system uses high pressure pumps to overcome the osmotic pressure and create more pressure on the thicker side of the solution.

Using mass and salt balance:

$$\dot{m}_{\mathrm{f}} = \dot{m}_{\mathrm{p}} + \dot{m}_{\mathrm{b}} \tag{26}$$

$$x_{\mathrm{f}}\dot{m}_{\mathrm{f}} = x_{\mathrm{P}}\dot{m}_{\mathrm{p}} + x_{\mathrm{b}}\dot{m}_{\mathrm{b}} \tag{27}$$

$\dot{m}_{\mathrm{f}}$, $\dot{m}_{\mathrm{p}}$ and $\dot{m}_{\mathrm{b}}$ are defined the feed water flow, penetration water flow rate, and salt water flow rate, and x_{P}, x_{f}, and x_{b} are feed salinity, penetration salinity, and salt salinity, respectively.

Feed water mass ratio is the ration of improved recovery R_{R} to fresh water mass flow rate $\dot{m}_{\mathrm{p}}$. Here R_{R} is considered 0.3 [53].

$$\dot{m}_{\mathrm{f}} = \frac{\dot{m}_{\mathrm{p}}}{R_{\mathrm{R}}} \tag{28}$$

The mass of water penetration through half-permeable membrane is defined as follows.

$$\dot{m}_{\mathrm{f}} = (\Delta P - \Delta\pi)K_W A_{\mathrm{W}} \tag{29}$$

In Eq. (29) A_{W} is parameters of the osmosis membrane area and K_{W} is water permeability coefficient.

$$K_{\mathrm{W}} = \frac{6.84 \times 10^{-8} \times \left(18.68 - \left(0.177 \times x_{\mathrm{b}}\right)\right)}{T_f} \tag{30}$$

In Eq. (30) the T_{f} parameter is the feed water temperature.

Pure mechanical power is expressed as follows.

$$W_{\mathrm{net}} = P_{\mathrm{F}} + P_{\mathrm{E}} \tag{31}$$

ΔP and $\Delta\pi$ are hydraulic penetration and osmotic pressure, respectively, as described below.

$$\Delta P = \overline{P} - P_{\mathrm{p}} \tag{32}$$

$$\Delta\pi = \overline{\pi} - \pi_{\mathrm{p}} \tag{33}$$

P_{p} and π_p are the hydraulic and osmotic pressures of the penetration flow, respectively. $\overline{P}$ and $\overline{\pi}$ are the average water pressure fed and the average osmotic pressure fed on the fed side and the saltwater side as follows:

$$\overline{P} = 0.5\left(P_{\mathrm{f}} + P_{\mathrm{b}}\right) \tag{34}$$

$$\overline{\pi} = 0.5\left(\pi_{\mathrm{f}} + \pi_{\mathrm{b}}\right) \tag{35}$$

P_{f} and P_{b} are hydraulic pressure of fed current and passed current, respectively. π_{f} and π_{b} are considered as osmotic pressure of fed current and passed current.

Osmotic pressures are defined as follows:

$$\pi_{\mathrm{f}} = \left(\mathrm{RTX}_{\mathrm{f}}\right) \tag{36}$$

$$\pi_{\mathrm{b}} = \left(\mathrm{RTX}_{\mathrm{b}}\right) \tag{37}$$

$$\pi_{\mathrm{p}} = \left(\mathrm{RTX}_{\mathrm{p}}\right) \tag{38}$$

R is measured as consonant global gases and T as water temperature and X_{f}, X_{b} and X_{p} are fed salinity, salt salinity and penetrating salinity, respectively.

In following equation ΔP_{net} is the efficiency of pure pressure passing from high pressure pump.

$$\Delta P_{\mathrm{net}} = \Delta P + \Delta\pi \tag{39}$$

Below equation $\dot{m}_{\mathrm{f}}$ shows output current rate from fresh water.

$$\dot{m}_{\mathrm{f}} = \frac{W_{\mathrm{net}}\rho_{\mathrm{f}}\eta_{\mathrm{pump}}}{\Delta P_{\mathrm{net}}} \tag{40}$$

ρ_{f} is fed current density rate and η_{pump} shows actuator pump mechanic efficiency.

Multi-objective optimization with evolutionary algorithms

Optimization algorithms

Genetic Algorithms were initially recommended by Prof. Holland (1960) by suggesting the notion of natural evolution and Darwinian formula for optimization goals [54]. The progress usually begins from people who unintentionally generated persons and happens in development. In every development, the fitness worth of every individual in the people is studied; multiple persons are adventitiously selected from the present people, and improved to make a new people. The new population is then used in the succeeding rehearsal of the GA. Typically, the GA stops once a satisfactory fitness level was attained for the people or majority of generations were made. Comprehensive explanations about GA can be seen in former literature [52].

Similarly, MOEAs were develop during the recent years by recurrent investigations on multiple mathematical puzzles and on applied engineering matters and have showed that they are able to ignore the difficulties of conventional methods [33, 51]. The structure of the MOEA used in this article is represented in Fig. 2 [36]. It is important to emphasize that the actual values of decision parameters were used instead of their binary coded.

NSGA-II approach

NSGA-II view was used in this article with the aim of showing the Pareto frontier by current GA. By the way, NSGA-II prepared the responses regarding the Pareto theory and arranging non-dominated responses into non-dominated layers as demonstrated in Fig. 3. In other words, if N_{p} signifies the population number, it is categorized to N_{L} layers wherein the interval of each two random selected layers is blank collection and mixture of all layers signifies N_{p} collection.

Virtual fitness of every response is the same as its layer. Tournament choice was used for crossover working in selecting parent between two accidental selected layers. Thus, response located on the first layer, have more chance to be selected for the next development. Uniform spreading of answers through layers is controlled through an index named "index of crowding distance" for every responses. This measure is demarcated as a ratio of detraction of objective purposes for two vicinage response close to the current

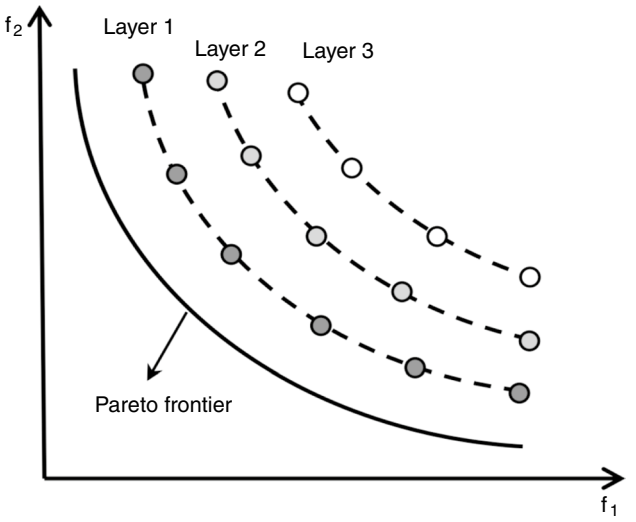

Fig. 3 NSGA-II solution layering [39–41]

answer to the reduction in the minimum and maximum values of that target. So, for k_{th} target of j_{th} response, below expression can be employed:

$$\dot{i}_{\mathrm{dis\,,\,j,\,k}} = \frac{f_{\mathrm{k\,,j\,-\,1}} - f_{\mathrm{k,\,j+1}}}{f_{\mathrm{k,max}} - f_{\mathrm{k,min}}} \tag{41}$$

For edge response are assigned to an unlimited interval index. The summary of individual interval values compatible to every target signifies the total crowding interval value like this:

$$I_{\mathrm{dis,\,j}} = \sum_{\mathrm{K-1}}^{M} i_{\mathrm{dis,j,k}} \tag{42}$$

where j stands for the individual index and M represents the number of objectives. Figure 4 shows a graphical image of analysis of distance index. In this method, two variables are considered for each response:

(1) Dominant (Layer) number, N_{L}, that is the number of response which regulate the existing response. Description and definitions of domination was defined properly in Ref. [55]. Dominant number, for non-dominated response of the existing population is the same as 0; therefore, these responses are placed in first layer. Non-dominated response for a collection of the responses not containing the first layer members are placed in second layer. For M targets issue with N people, the number of considerations is the same as MN^2. This procedure carry on with the aim of accommodating all responses in their proper layers. Additionally, i rank index for every response is assigned as its layer number, N_{L}.

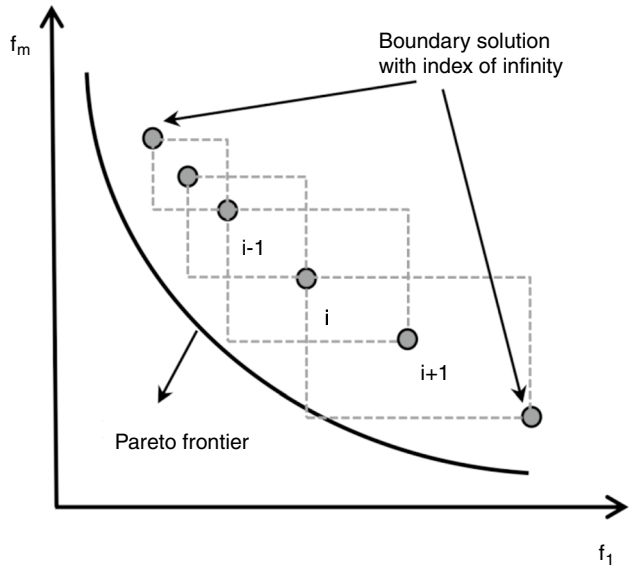

Fig. 4 Schematic of Distance indexing of components in NSGA-II algorithms [39–41]

(2) Crowded comparison operator, $n\prec$, demarcated as following as:

$$A \prec B \text{if}(\text{rank}_A < \text{rank}_B)$$
$$\text{or}: \quad (43)$$
$$((\text{rank}_A = \text{rank}_B)\text{and}I_{\text{dis,A}} > I_{\text{dis,B}})$$

It shows that for two responses that have different layers, the response with the lower layer is preferred. Also, for two responses of the similar layer, the answer positioned in the area with lower concentration of answers is selected.

Decision-making in the multi-objective optimization

Selecting an ending optimum response from Pareto optimal frontier in multi-objective optimization procedure has an important part. Therefore, we must use decision makers to define this. Therefore, in this article three proficient decision makers comprising TOPSIS, Fuzzy and LINMAP were used as decision makers. More information of these decision makers could be seen in former works specifically references [53, 54, 56, 57].

Results and discussion

In the results and discussion of this article, three main scenarios are suggested to simulate the presented system. In the first scenario evaluate the hybrid system inclusive the power ($P=100\%$) and the fresh water production ($m_f=0$). Therefore, present hybrid system investigates the variation of the power, efficiency, exergy efficiency, exergy destruction density and, thermo-environmental function with current density according to Figs. 5–9. In the second scenario consider the hybrid system inclusive the power ($P=50\%$) and the fresh water production ($m_f=50\%$). So the present hybrid system considers the fresh water production with a current density that the maximum fresh water production (m_f) is 1.2 kg s^{-1} according to Fig. 10. In the third scenario investigate the hybrid system inclusive the fresh water production ($m_f=100\%$) and the power ($p=0$). Nevertheless, the present hybrid system considers variation of the fresh water production with current density in different temperatures and the maximum fresh water production (m_f) is 2.5 kg s^{-1}, as shown in Fig. 11. Optimization aims to increase the fresh water production, according to the three tables which are covering

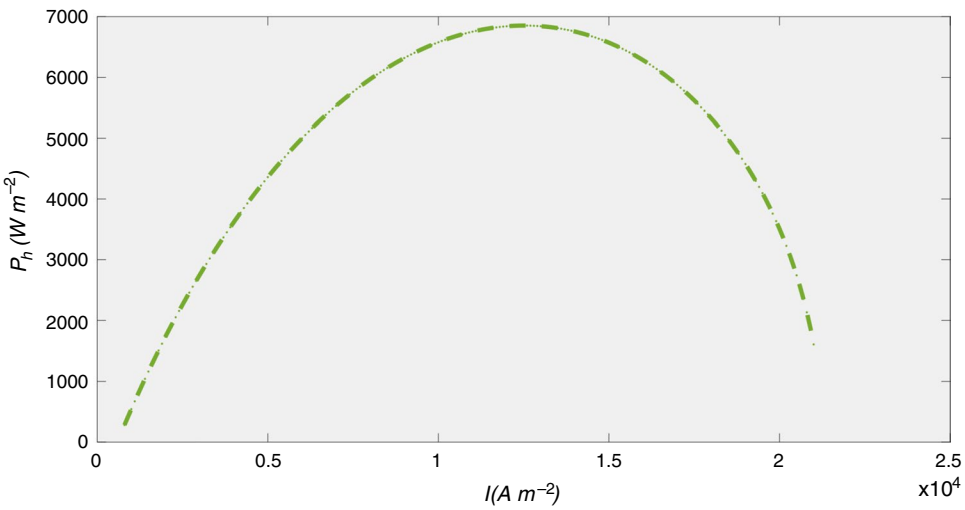

Fig. 5 Evaluation of the effect of current density on power

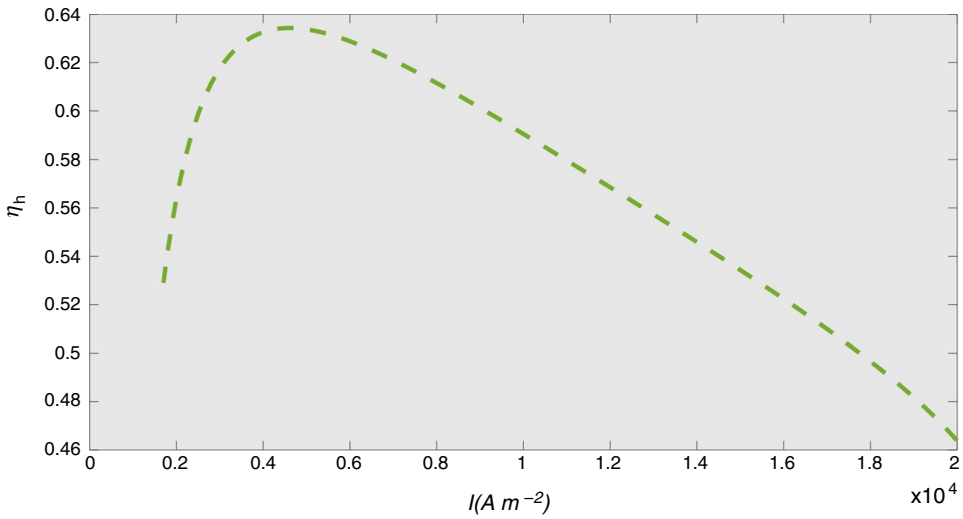

Fig. 6 Evaluation of the effect of current density on efficiency

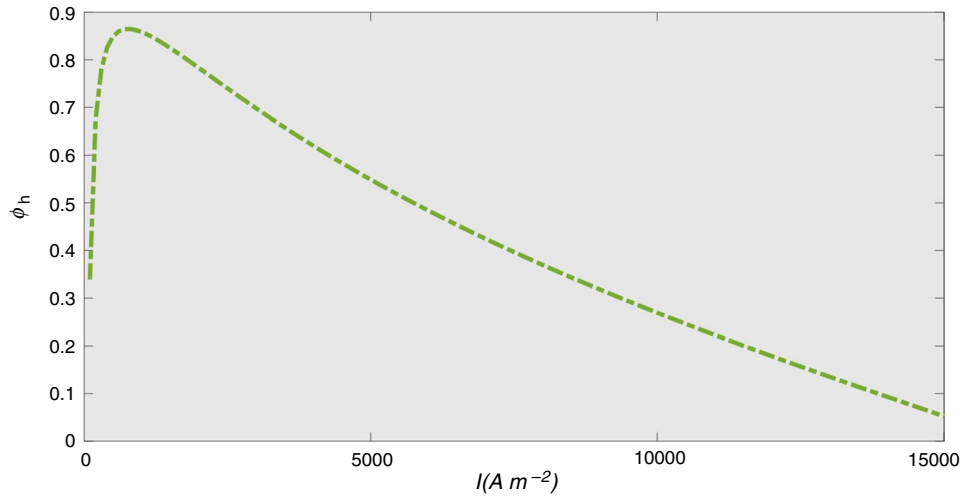

Fig. 7 Evaluation of the effect of current density on exergy efficiency

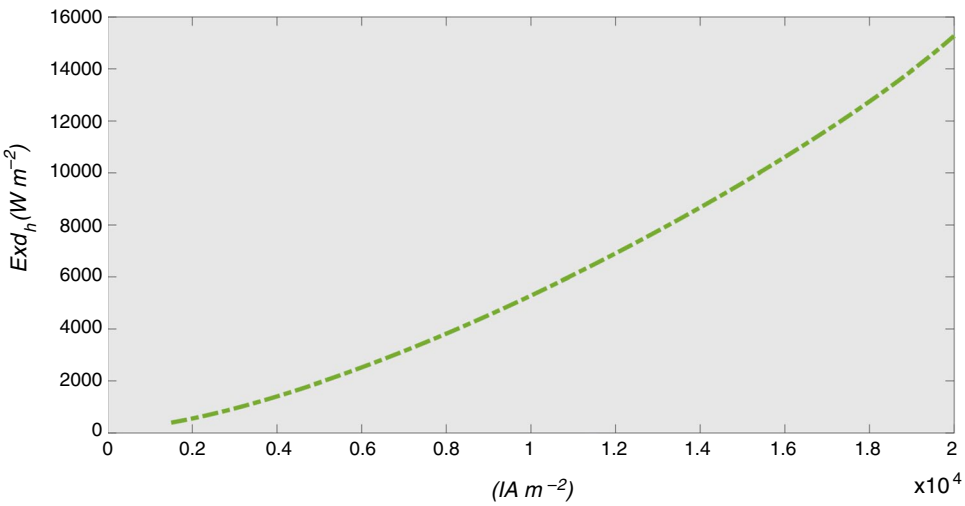

Fig. 8 Evaluation of the effect of current density on exergy destruction density

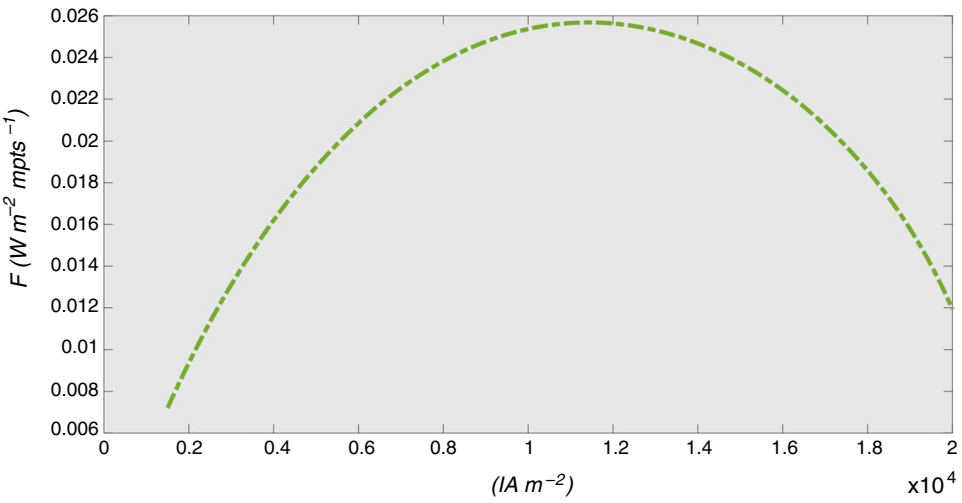

Fig. 9 Evaluation of the effect of current density on thermo-environmental function density

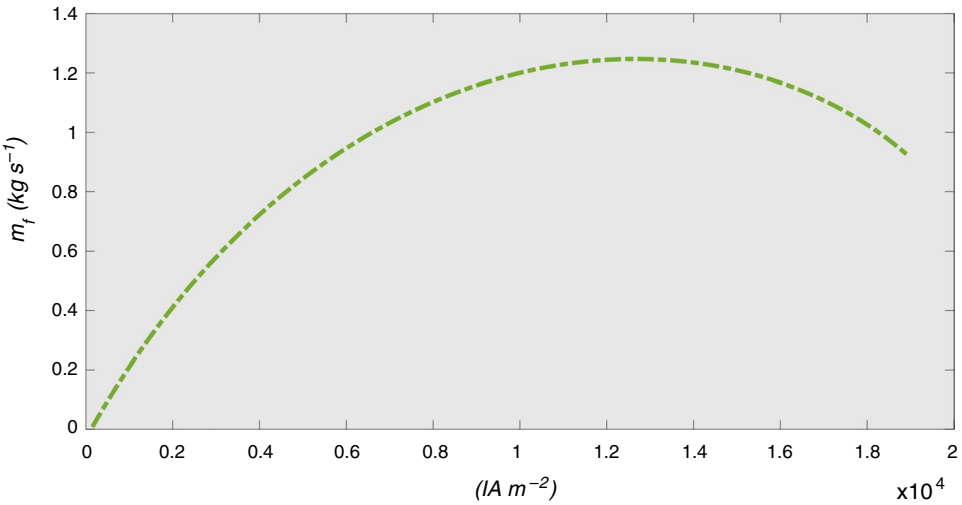

Fig. 10 Evaluation of the effect of current density on mass flow

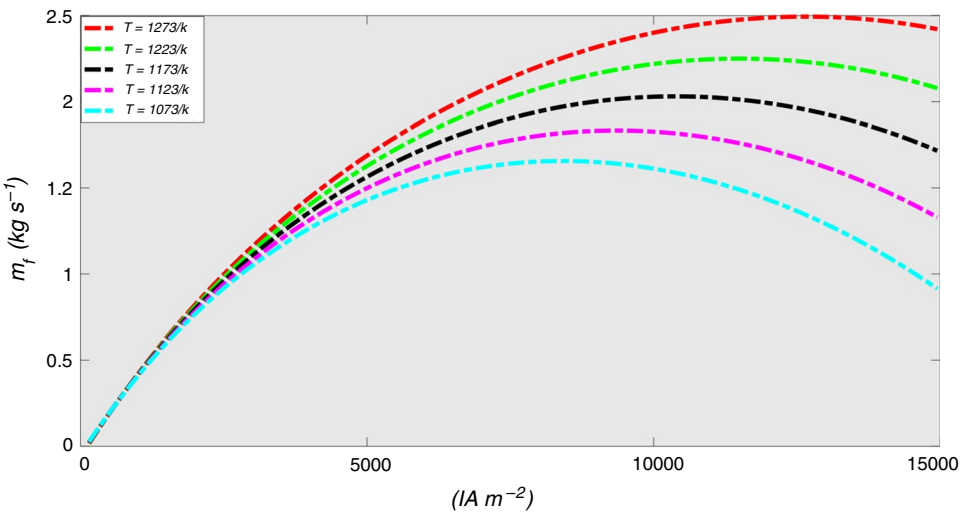

Fig. 11 Evaluation of mass flow with different temperature at different current density

optimization results, the first table has the maximum fresh water production is in FUZZY that it is $m_f = 2.078$.

The first scenario simulates the hybrid system with power ($P = 100\%$) and the fresh water production ($m_f = 0$), as well as the effect of power on other parameters of the hybrid system, such as efficiency (η_h), exergy destruction density (Exd_h), energy efficiency and exergy (ϕ_h) and thermo-environmental function (F) have been investigated.

According to Fig. 5, as current density increases, the output power of the hybrid system firstly rise and after that reduced. Since via increasing current density, system losses similarly increase; therefore rise waste decreases the output voltage of the hybrid system and then reduces power, but since initially, the voltage is high, the power will increase in the first phase, then with an extra reduction in the voltage, the output power of the hybrid system will reduce too. As the figure shows, in the current $i = 12{,}600$ A m^{-2}, the maximum output power of the hybrid system is $P_h = 6852$ W m^{-2}.

According to Fig. 6, as the current density increases, hybrid system efficiency at first rise and later reduced. Since by increasing current density, system losses will increase as well, thus, losses increasing result in decrease in output voltage and therefore result in decrease in hybrid system efficiency; however due to having high voltage in the beginning, hybrid system efficiency will increase at first phase and after that by further decrease in voltage, hybrid system efficiency will reduce too. According to figure in current density $i = 4700$ A m^{-2}), the maximum value is $\eta_h = 0/6343$ (A m^{-2}).

Figure 7 demonstrates which, by increasing current density, the exergy efficiency and charts of the hybrid system initially increase and after that decrease. As the system's current loss increases with increasing density, increasing the loss decreases the hybrid system's voltage and therefore decreases exergy efficiency. Then since the voltage is high initially, the energy efficiency of the hybrid system increases in the initial phase, after that the energy efficiency of the hybrid system similarly reduces with more decrease in voltage. As the maximum figure shows, the energy efficiency at the current density $i = 690$ A m^{-2} is $\phi_h = 91/39$.

According to shape 4, the direct effect of current density on the exergy destruction density at the beginning of the shape; according to earlier diagrams, increasing current density is related with increasing losses and increasing losses is a form of thermodynamic destruction for the system. Consequently, increasing the current density similarly increases exergy destruction density. In this shape, the maximum current density of the current i = 19,000 A m^{-2} is the exergy destruction density equal to Exd = 12,240 W m^{-2}.

According to shape 5, by increasing current density the environmental function thermistor initially increases and then reduces. Since increase in the current density, causes increase the loss and voltage and then decrease the voltage, and reducing the voltage impacts all system performance, comprising power, efficiency, exergy failure density, in addition to the environmental thermostat function, but as the system voltage is low in the beginning hybrids have a high volume of environmental thermocouple function. As presented in the figure, at the current density of $i = 11{,}700$ A m^{-2}, the maximum value of the exergy destruction density is $F = 0.02567$ W m^{-2}.

In the second scenario, the performance of the hybrid system with the power ($P = 50\%$) and fresh water production ($m_f = 50\%$) are examined. At this stage, by receiving 50% of the power and 50% of the fresh water flow, the behavior of the fresh water flow diagram (m_f) has been investigated.

As Fig. 10 shows, the increase in the current density causes increase in freshwater flow initially and after that decreases, since as the density increase, the flow of losses increases and the increase in losses decreases the voltage. Decrease in the voltage causes reduce in the total power of the system and hence decreases the fresh water flow. Since the voltage is high initially, the power of the system and the flow rate of fresh water increase as well, however, with more reduction in voltage, the power of the system and the extent of flow rate of fresh water reduces since consistent with Eq. 40, fresh water flow has a direct relationship with power.

In the third scenario, the simulation of the system provided with the fresh water production ($m_f = 100\%$) and the power ($P = 0$) is examined. At this stage, the total freshwater flow received by the current density was evaluated at different temperatures.

According to Fig. 11, in a constant current density, the extent of the fresh water production (m_f) increases by increasing temperature, the reason is that the fresh water production rate is directly associated with the output power of the system and the output power of the system is associated with temperature. Accordingly, the extent of the fresh water production (m_f) increases. Moreover, at a constant temperature, by increase in flow density, the fresh water production (m_f) firstly increases and after that reduces, since by increasing flow density, the extent of losses increases and increasing the losses causes decrease in the voltage, after that since the voltage has a high value initially, it causes increase in the system power. Therefore, the flow of the fresh water production has increased, but as the voltage reduces, the flow rate decreases as well.

The optimal beam frontier for the first scenario is demonstrated in Fig. 12, and also the optimal points, such as TOPSIS, FUZZY and LINMAP specified on the figure.

The optimal beam frontier for the second scenario is illustrated in Fig. 13, and also the optimal points, such as TOPSIS, FUZZY and LINMAP specified on the figure.

The optimal beam frontier for the third scenario is illustrated in Fig. 14, and also the optimal points, such as TOPSIS, FUZZY and LINMAP specified on the figure.

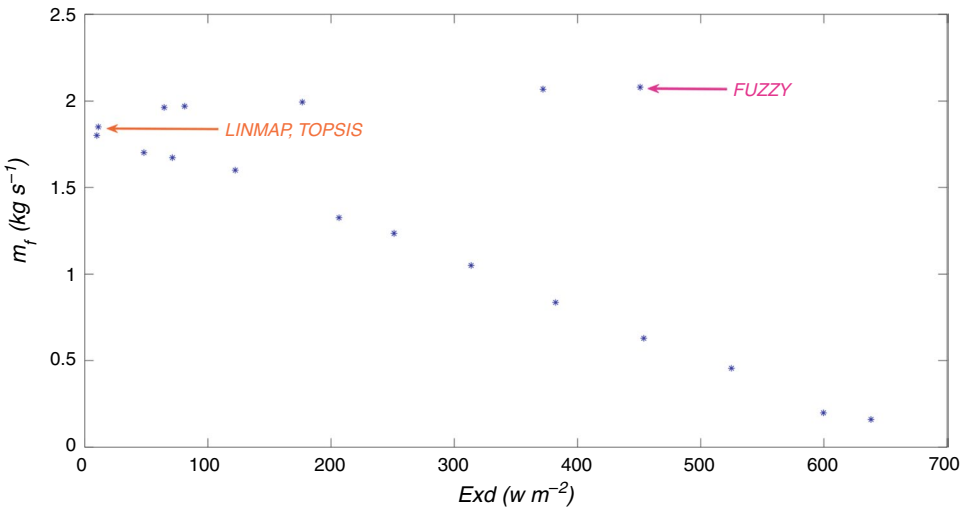

Fig. 12 Pareto optimal front for the first scenario

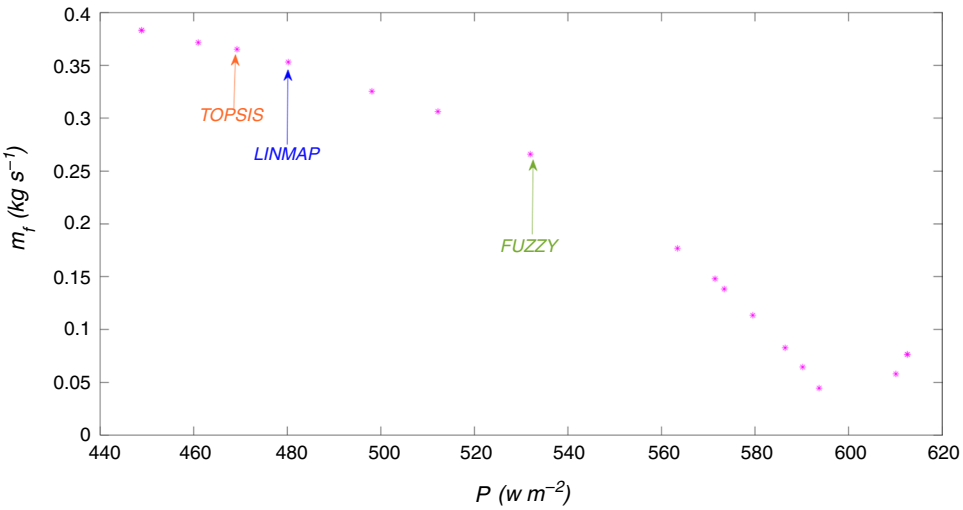

Fig. 13 Pareto optimal front for the second scenario

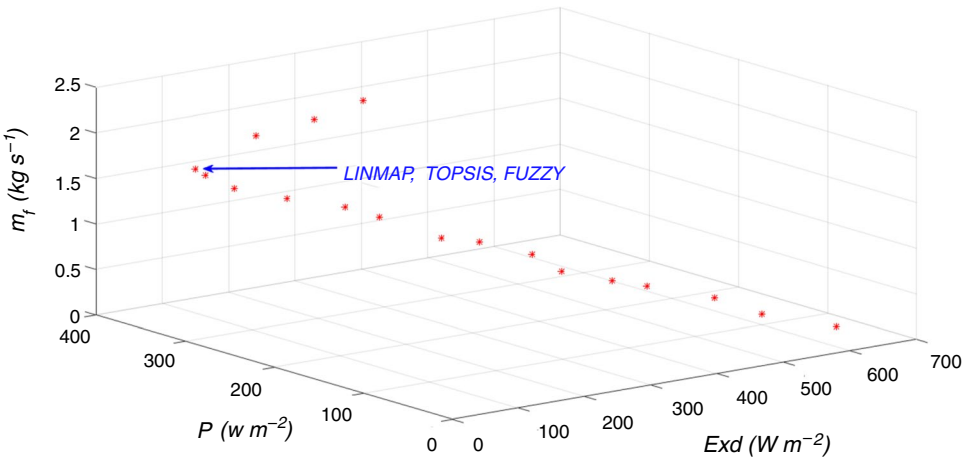

Fig. 14 Pareto optimal front for the third scenario

Numerical results obtained from performance three methods, TOPSIS, LINMAP, and FUZZY for the first scenario are presented in Table 1.

Numerical results obtained from performance three methods, TOPSIS, LINMAP, and FUZZY for the second scenario are presented in Table 2.

Table 1 Outcomes of the decision methods for the first scenario

Decision variable	m_f /kg s^{-1}	Exd /w m^{-2}	I /A m^{-2}	T /k	A /m^2	P_C /kw
TOPSIS	1.85033113	11.0138186	8230.873	1110.177	0.756859	6640.2
LINMAP	1.85033113	11.0138186	8230.873	1110.177	0.756859	6640.2
FUZZY	2.07894417	450.879301	11,139.04	1103.741	0.799981	9084.7

Table 2 Outcomes of the decision methods for the second scenario

Decision variable	P /kw	m_f /kg s^{-1}	I /A m^{-2}	T /k	A /m^2	Exd_C /w m^{-2}
TOPSIS	469.252609	0.36526481	13,522.1	1073.011	0.799685	13,223
LINMAP	480.21189	0.3531284	13,811.44	1073.012	0.799626	13,696
FUZZY	531.965487	0.2661149	15,256.12	1073.005	0.799938	16,176

Table 3 Outcomes of the decision methods for the third scenario

Decision variable	P /kw	m_f /kg s^{-1}	Exd /w m^{-2}	I /A m^{-2}	T /k	A /m^2
TOPSIS	311.105584	1.81689324	30.4398967	8484.765	1130.71	0.749749
LINMAP	311.105584	1.81689324	30.4398967	8484.765	1130.71	0.749749
FUZZY	311.105584	1.81689324	30.4398967	8484.765	1130.71	0.749749

Table 4 Outcomes maximum and average error of the decision methods for the first scenario

Amount	TOPSIS		LINMAP		FUZZY	
	Exd	m_f	Exd	m_f	Exd	m_f
MAX (%)	66.60	13.14	66.60	13.14	49.86	4.49
Average (%)	41.86	8.12	41.86	8.12	27.9	3.95

Table 5 Outcomes maximum and average error of the decision methods for the second scenario

Amount	TOPSIS		LINMAP		FUZZY	
	P	m_f	P	m_f	P	m_f
MAX (%)	1.67	2.041	2.1056	2.77	2.59	13.386
Average (%)	0.925	1.33	1.377	2.047	1.88	8.087

Numerical results obtained from performance three methods, TOPSIS, LINMAP, and FUZZY for the third scenario are presented in Table 3.

As shown in Table 4, the error analysis results (maximum error and average error) are presented for optimization results, which is based on the results obtained from TOPSIS and LINMAP for the maximum error. Also, the maximum error for the optimal exergy destruction exergy is related to (TOPSIS, LINMAP).

As shown in Table 5, the error analysis results (maximum error and average error) are presented for optimization results, which is based on the results obtained from FUZZY for the maximum error. Also, the maximum error for the amount of mass flow rate (m_f) is interacted to (FUZZY).

As shown in Table 6, the error analysis results (maximum error and average error) are presented for optimization results, which is equal for all cases (LINMAP, TOPSIS, FUZZY).

Table 6 Outcomes maximum and average error of the decision methods for the third scenario

Amount	TOPSIS			LINMAP			FUZZY		
	P	m_f	Exd	P	m_f	Exd	P	m_f	Exd
MAX (%)	6.91	6.911	34.05	6.91	6.911	34.05	6.91	6.911	34.05
Average (%)	4.905	4.91	26.205	4.905	4.91	26.205	4.905	4.91	26.205

Conclusions

This paper provides a detailed thermodynamic analysis to evaluate the performance of a hybrid system, including a solid oxide fuel cell (SOFC)–Ericsson heat engine–reverse osmosis desalination (RO). In this study investigate the Ericsson heat engine and incorporate it with solid oxide fuel cell (SOFC), furthermore consider parameters power (P), efficiency (η), exergy efficiency (ϕ), and exergy destruction density (Exd). Evaluate double two-objective optimization operations and a three-objective optimization operation, each of which involves a combination of objective functions. To select the final results from Pareto fronts, three prominent decision-making methods LINMAP, TOPSIS, FUZZY have been used. The first scenario includes optimization of the exergy destruction density and fresh water production. The exergy destruction density has suit condition in the FUZZY approach which it values equal is 450.879 (W m^{-2}); the fresh water production also has the highest value in FUZZY which is 2.078 (kg s^{-1}). In the second scenario consider optimization of the power (P) and fresh water production (m_f). The power has a better condition in FUZZY that the value is 531.965; the fresh water production achieves maximum value in TOPSIS that it value its 0.365 (kg s^{-1}). In the third scenario that includes the power (P), the fresh water production (m_f), and exergy destruction density (Exd). The power has equal value in three decision-making that it value is 311.105 (KW); also the fresh water production has a constant value in three decision-making that it is 1.816 (kg s^{-1}); the exergy destruction density in three decision-making has an equal value that is 30.439 (W m^{-2}). In the first scenario, the least maximum error and the average error of the exergy destruction density is in the FUZZY method, which it error values are 49.86% and 27.9%, respectively; the fresh water production has the least maximum error and the average error in the FUZZY result, which it error values are 4.49 and 3.95, respectively. In the second scenario, the lowest maximum error and the average error of the power are in TOPSIS methods, which the values are, respectively, 1.67 and 0.925; the fresh water production has the lowest maximum error and the average error in TOPSIS result, that the lowest maximum is 2.041 and the least average is 1.330. In the third scenario, the maximum error of power is equal in three decision-making methods which the numerical value is 6.91, also the average error of the power is equal in three decision-making methods that the is 4.905; the maximum error of fresh water production is 6.911 in three decision-making methods and the average error of fresh water production is 4.91 in three decision-making methods. The maximum error of exergy destruction density has equal value in three decision-making methods that is 34.05 and the average error of exergy destruction density is 26.205 in three decision-making methods.

References

1. Grisolia G, Fino D, Lucia U. ofuThermodynamic optimisation of the biel production based on mutualism. Energy Rep. 2020;6:1561–71.
2. U. Lucia, D. Fino, and G. Grisolia, "Thermoeconomic analysis of Earth system in relation to sustainability: a thermodynamic analysis of weather changes due to anthropic activities. J. Therm. Anal. Calorim. 2020.
3. A. Arabkoohsar and M. Sadi, "Thermodynamics, economic and environmental analyses of a hybrid waste–solar thermal power plant," *J. Therm. Anal. Calorim.*, no. 0123456789, 2020.
4. Nesaraj AS. Recent developments in solid oxide fuel cell technology—A review. J Sci Ind Res (India). 2010;69(3):169–76.
5. Gebregergis A, Pillay P, Bhattacharyya D, Rengaswemy R. Solid Oxide Fuel Cell Modeling. IEEE Trans Ind Electron. 2009;56(1):139–48.
6. RA Rasid, A Nafees Study of natural gas powered solid oxide fuel cell simulation and modelling. In: IOP Conf. Ser. Mater. Sci. Eng., vol. 702, no. 1, 2019.
7. Gauckler LJ, et al. Solid oxide fuel cells: systems and materials. Chimia (Aarau). 2004;58(12):837–50.
8. A. Lanz, J. Heffel, and C. Messer, "Hydrogen Fuel Cell Engines—Introduction," *Fuel Cell Technol.*, no. September, p. 53, 2001.
9. Zaccaria V, Tucker D, Traverso A. Gas turbine advanced power systems to improve solid oxide fuel cell economic viability. J Glob Power Propuls Soc. 2017;1:U96IED.
10. Irshad M, et al. A brief description of high temperature solid oxide fuel cell's operation, materials, design, fabrication technologies and performance. Appl Sci. 2016;6(3):75.
11. Su S, Gao X, Zhang Q, Kong W, Chen D. Anode—versus cathode-supported solid oxide fuel cell : effect of cell design on the stack performance. Int J Electrochem Sci. 2015;10:2487–503.
12. Beigzadeh M, Pourfayaz F, Ahmadi MH, Pourkiaei SM, Beigzadeh M. A Simplificative Approach-based Modeling of SOFC Power Systems Fed by Natural Gas. Fuel Cells. 2017;17(6):843–53.
13. Zhao Y, Ou C, Chen J. A new analytical approach to model and evaluate the performance of a class of irreversible fuel cells. Int J Hydrogen Energy. 2008;33(15):4161–70.

14. Açıkkalp E. Thermo-environmental performance analysis of irreversible solid oxide fuel cell–Stirling heat engine. Int J Ambient Energy. 2018;39(7):751–8.
15. Xu H, et al. Performance improvement of a direct carbon solid oxide fuel cell through integrating an Otto heat engine. Energy Convers Manag. 2018;165:761–70.
16. Zhang X, Wang Y, Guo J, Shih TM, Chen J. A unified model of high-temperature fuel-cell heat-engine hybrid systems and analyses of its optimum performances. Int J Hydrogen Energy. 2014;39(4):1811–25.
17. Zhang X, Chen J. Performance analysis and parametric optimum criteria of a class of irreversible fuel cell/heat engine hybrid systems. Int J Hydrogen Energy. 2010;35(1):284–93.
18. Zhang X, Su S, Chen J, Zhao Y, Brandon N. A new analytical approach to evaluate and optimize the performance of an irreversible solid oxide fuel cell-gas turbine hybrid system. Int J Hydrogen Energy. 2011;36(23):15304–12.
19. Zhang X, Guo J, Chen J. Influence of multiple irreversible losses on the performance of a molten carbonate fuel cell-gas turbine hybrid system. Int J Hydrogen Energy. 2012;37(10):8664–71.
20. Chen L, Gao S, Zhang H. Performance analysis and multi-objective optimization of an irreversible solid oxide fuel cell-stirling heat engine hybrid system. Int J Electrochem Sci. 2013;8(8):10772–87.
21. Gholamian E, Hanafizadeh P, Ahmadi P. Exergo-economic analysis of a hybrid anode and cathode recycling SOFC/Stirling engine for aviation applications. Int J Sustain Aviat. 2018;4(1):11.
22. Rokni M. Thermodynamic analysis of SOFC (solid oxide fuel cell)-Stirling hybrid plants using alternative fuels. Energy. 2013;61:87–97.
23. Rokni M. Thermodynamic and thermoeconomic analysis of a system with biomass gasi fi cation, solid oxide fuel cell (SOFC) and Stirling engine. Energy. 2014;76:19–31.
24. Mehrpooya M, Sadeghzadeh M, Rahimi A, Pouriman M. Technical performance analysis of a combined cooling heating and power (CCHP) system based on solid oxide fuel cell (SOFC) technology—A building application. Energy Convers Manag. 2019;198:111767.
25. Tyagi SK, Kaushik SC, Salhotra R. Ecological optimization and performance study of irreversible Stirling and Ericsson heat engines. J Phys D Appl Phys. 2002;35(20):2668–75.
26. Chen J, Schouten JA. The comprehensive influence of several major irreversibilities on the performance of an Ericsson heat engine. Appl Therm Eng. 1999;19(5):555–64.
27. Hachem H, et al. Comparison based on exergetic analyses of two hot air engines: a Gamma type Stirling engine and an open joule cycle Ericsson engine. Entropy. 2015;17(11):7331–48.
28. Komninos NP, Rogdakis ED. Design considerations for an Ericsson engine equipped with high-performance gas-to-gas compact heat exchanger: a numerical study. Appl Therm Eng. 2018;133:749–63.
29. Ngangué MN, Stouffs P. Dynamic simulation of an original Joule cycle liquid pistons hot air Ericsson engine. Energy. 2020;190:116293.
30. Fula A, Stouffs P, Sierra F. In-cylinder heat transfer in an ericsson engine prototype. Renew Energy Power Qual J. 2013;1(11):1260–5.
31. Bădescu V. Optimum operation of a solar converter in combination with a Stirling or Ericsson heat engine. Energy. 1992;17(6):601–7.
32. Erbay LB, Yavuz H. Analysis of an irreversible Ericsson engine with a realistic regenerator. Appl Energy. 1999;62(3):155–67.
33. Ďurčanský P, Lenhard R, Jandačka J. Heat exchanger design for hot air ericsson-brayton piston engine. EPJ Web Conf. 2016;67(April):2014.
34. E. Kussul, O. Makeyev, T. Baidyk, J. S. Blesa, and N. Bruce, "Ericsson heat engine with microchannel recuperator for solar concentrator with flat mirrors," vol. 6, no. 4, 2012.
35. P. Cedex, F. Corresponding, and P. Stouffs, "Dynamic simulation of a small Joule cycle Ericsson engine: first results," In: Int. Stirling Forum 2008, no. September, p 10, 2008.
36. Ahmadi MH, Hosseinzade H, Sayyaadi H, Mohammadi AH, Kimiaghalam F. Application of the multi-objective optimization method for designing a powered Stirling heat engine: Design with maximized power, thermal efficiency and minimized pressure loss. Renew Energy. 2013;60:313–22.
37. Ahmadi MH. Thermo-environmental analysis and multi-objective optimization of performance of ericsson engine implementing an evolutionary algorithm. J Therm Eng. 2019;5(4):319–40.
38. Punnathanam V, Kotecha P. Multi-objective optimization of Stirling engine systems using Front-based yin-yang-pair optimization. Energy Convers Manag. 2017;133:332–48.
39. Ahmadi MH, Ahmadi MA, Mehrpooya M, Pourkiaei SM, Khalili M. Thermodynamic analysis and evolutionary algorithm based on multi-objective optimisation of the Rankine cycle heat engine. Int J Ambient Energy. 2016;37(4):363–71.
40. Ahmadi MH, Ahmadi MA, Pourfayaz F, Bidi M, Açikkalp E. Multi-objective optimization and exergetic-sustainability of an irreversible nano scale Braysson cycle operating with Ma xwell-Boltzmann gas. Alexandria Eng J. 2016;55(2):1785–98.
41. Ahmadi MH, Alhuyi Nazari M, Feidt M. Thermodynamic analysis and multi-objective optimisation of endoreversible Lenoir heat engine cycle based on the thermo-economic performance criterion. Int J Ambient Energy. 2019;40(6):600–9.
42. Behzadi Forough A, Roshande R. Multi objective optimization of solid oxide fuel cell stacks considering parameter effects: fuel utilization and hydrogen cost. Renew Sustain Energy. 2013;5(5):053124.
43. X. Wu, L. He, D. Gao, and Y. Zhu 2019 Multi-objective optimization of SOFC systems. In: IOP Conf. Ser. Earth Environ. Sci., vol. 257, no. 1, 2019.
44. Salehi Z, Gholaminezhad I. Multi-objective modeling, uncertainty analysis, and optimization of reversible solid oxide cells. Int J Energy Environ Eng. 2018;9(3):295–304.
45. Quddus MR, Zhang Y, Ray AK. Multi-objective optimization in solid oxide fuel cell for oxidative coupling of methane. Chem Eng J. 2010;165(2):639–48.
46. Khani L, Mehr AS, Yari M, Mahmoudi SMS. Multi-objective optimization of an indirectly integrated solid oxide fuel cell-gas turbine cogeneration system. Int J Hydrogen Energy. 2016;41(46):21470–88.
47. Ahmadi MH, Jokar MA, Ming T, Feidt M, Pourfayaz F, Astaraei FR. Multi-objective performance optimization of irreversible molten carbonate fuel cell–Braysson heat engine and thermodynamic analysis with ecological objective approach. Energy. 2018;144(2018):707–22.
48. R. S. V Selladurai, Á. R. Cop, and R. Á. Efficiency, "Exergy analysis of a domestic refrigerator using eco-friendly R290/R600a refrigerant mixture as an alternative to R134a," 2013.
49. M. Senturk and A. Oguz, "Energy and exergy analysis of solar energy-integrated , geothermal energy-powered Organic Rankine Cycle.J Therm Anal Calorim 2019.
50. Murugapoopathi S. Energy and exergy analysis on variable compression ratio multi-fuel engine. J Therm Anal Calorim. 2018;136:255–66.
51. Vakilabadi MA, Najafi MBAF, Hossein M. Energy, Exergy analysis and performance evaluation of a vacuum evaporator for solar thermal power plant zero liquid discharge systems. J Therm Anal Calorim. 2019;139:1275–90.
52. Alijanpour M, Seyed S, Mousavi S, Mojtaba A, Delavar A. Thermodynamic analysis of waste heat recovery from hybrid system

of proton exchange membrane fuel cell and vapor compression refrigeration cycle by recuperative organic Rankine cycle. J Therm Anal Calorim. 2018;135:1699–712.
53. Xia G, Sun Q, Cao X, Wang J, Yu Y, Wang L. Thermodynamic analysis and optimization of a solar-powered transcritical CO2 (carbon dioxide) power cycle for reverse osmosis desalination based on the recovery of cryogenic energy of LNG (liquefied natural gas). Energy. 2014;66:643–53.
54. Konak A, Coit DW, Smith AE. Multi-objective optimization using genetic algorithms: a tutorial. Reliab Eng Syst Saf. 2006;91(9):992–1007.
55. E. Chattoe, "Modeling economic interaction using a genetic algorithm," Handb. Evol. Comput., no. September, 2004.
56. Mazur V. Fuzzy thermoeconomic optimization of energy-transforming systems. Appl Energy. 2007;84(7–8):749–62.
57. Olson DL. Decision aids for selection problems. J Oper Res Soc. 1997;48(5):541–2.